World Electric Vehicle Journal

MDPI

Article

Resilience-Oriented Predictive Energy Management and Route Adaptation for Long-Distance Electric Vehicles Under Charging Infrastructure and Road Network Uncertainties

Bilal Khan [1,2], Zahid Ullah [3,4], Giambattista Gruosso [3,*] and Salman Habib [1,5]

[1] Control and Instrumentation Department, King Fahd University of Petroleum and Minerals, Dhahran 31261, Saudi Arabia; salman.habib@kfupm.edu.sa (S.H.)
[2] Center for Sustainable Energy Systems (IRC-SES), King Fahd University of Petroleum & Minerals, Dhahran 31261, Saudi Arabia
[3] Dipartimento di Elettronica, Informazione e Bioingegneria, Politecnico di Milano, 20133 Milan, Italy
[4] Faculty of Electrical Engineering, Ghulam Ishaq Khan Institute of Engineering Sciences and Technology, Topi 23640, Pakistan
[5] Center for Smart Mobility and Logistics (IRC-SML), King Fahd University of Petroleum & Minerals, Dhahran 31261, Saudi Arabia
* Correspondence: giambattista.gruosso@polimi.it

Abstract

The increased deployment of electric vehicles (EVs) has increased the demand for intelligent energy management strategies to ensure reliable and efficient operation during long-distance travel. Existing EV energy management methods are mainly concerned with energy optimization of the batteries and charging scheduling; however, they often assume reliable charging infrastructure and fixed travel routes. In real-world environments, charging stations can be congested, unavailable, or out of service, and traffic incidents and road closures can affect route feasibility and energy usage. These uncertainties may lead to energy depletion (vehicle stranding) and may compromise successful trip completion. Therefore, this paper proposes a resilience-oriented predictive energy management and route-adaptation framework for long-distance EVs operating under uncertainties in charging infrastructure and the transportation network. The proposed unified decision-making framework incorporates the ability to predict the battery state of charge, estimate the energy requirement of an EV, and determine the availability of charging stations, traffic conditions, disruptions in the road network, and regenerative energy recovery opportunities. A safety-constrained predictive controller is developed to dynamically manage energy consumption while maintaining a minimum energy reserve that guarantees access to feasible charging alternatives under adverse operating conditions. Further, real-time route adaptation is achieved via continuous monitoring of charging station conditions, projected wait times, and road network conditions to determine the most energy-efficient and resilient routes. To assess operational robustness, a resilience index is introduced to quantify the vehicle's capability to complete a trip while satisfying energy safety constraints in the presence of infrastructure and traffic disturbances. Monte Carlo simulation results on a representative long-distance corridor demonstrate that the proposed framework achieves a 99.3% mission success rate versus 67.3% for a naive shortest-distance baseline, while reducing generalized operating costs by 21.5% and charging stops by 42% relative to a conservative full-charge baseline. These results are simulation-based case study outcomes for the representative corridor and disturbance model studied here and are not measured or expected real-world performance. The proposed approach provides a practical pathway toward resilient, intelligent, and reliable next-generation electric mobility systems.

Check for updates

Academic Editor: Michael Fowler

Received: 28 July 2026
Revised: 28 August 2026
Accepted: 29 August 2026
Published: 31 August 2026

Copyright: © 2026 by the authors. Published by MDPI on behalf of the World Electric Vehicle Association. Licensee MDPI, Basel, Switzerland. This article is an open access article distributed under the terms and conditions of the Creative Commons Attribution (CC BY) license.

Keywords: electric vehicles; resilience-oriented control; predictive energy management; route adaptation; charging infrastructure uncertainty

1. Introduction

The transition toward electric vehicles (EVs) is reshaping long-distance road travel, but it also reintroduces a constraint that conventional internal combustion vehicles largely avoided. A trip's feasibility now depends on the availability of external infrastructure en route, not only on the vehicle's own fuel reserve. A gasoline vehicle can typically find refueling options within minutes almost everywhere, whereas an EV on a multi-hour corridor trip may depend on a small number of DC fast-charging stations, each of which can be congested, temporarily out of service, or slower than expected. Field studies of public charging networks report meaningful shares of chargers being non-operational or degraded at any given time. The network-level analyses show that the failure of even a handful of charging stations can materially reduce the reachability of an electrified road corridor [1]. Traffic incidents and road network disruptions compound this problem by changing both travel time and energy consumption along a planned route. Consequently, energy management [2] and routing decisions for long-distance EV travel cannot be treated as independent, one-shot planning problems solved under nominal conditions. This problem must be treated as a coupled, uncertainty-aware decision process that adapts as conditions change.

Existing work addresses parts of this problem in isolation [3]. Energy-optimal EV routing has been studied extensively as an extension of classical shortest-path algorithms, adapted to handle the negative edge costs introduced by regenerative braking and the path-dependence introduced by battery capacity limits [4,5]. Reachability-aware routing further formalizes the question of whether a destination (or a charging station) can be reached at all without exhausting the battery and introduces the option of en-route charging, typically under the simplifying assumption that the vehicle recharges to full capacity whenever it stops [6]. This latter approach relaxes this assumption by choosing more optimal partial charging quantities based on the continuous state-of-charge profiles [7]. Although these algorithms are very efficient, they are essentially deterministic and offline. They are computing one route with a fixed known network and charger state, and do not update the computed route as the actual conditions change. Battery power allocation, regenerative braking, and degradation-aware control in a receding-horizon loop [8] are all part of the energy management of an EV, which can be handled by model predictive control (MPC) [3] separately. This body of work, however, usually assumes that the path is known and does not assign the energy controller to a particular routing decision that can be rerouted online.

To address the gap, this paper introduces an online dynamic resilience-oriented predictive energy management and route adaptation (REM-RA) framework that incorporates the stochastic nature of charger availability, traffic conditions, and road accessibility. The model ensures safe margins against energy exhaustion with explicit constraints and chance constraints, which are continually adjusted as the online state is updated, both spatially and in terms of energy management strategies. In this regard, the paper proposes a resilience-oriented predictive energy management and route-adaptation (REM-RA) framework that (a) models the EV as a hybrid cyber-physical system coupling battery energy and health dynamics, vehicle longitudinal dynamics, and a stochastic infrastructure state; (b) defines a resilience margin directly in terms of the set of charging stations reachable without violating a minimum SoC bound and enforces it as a state-dependent, chance-constrained requirement rather than a soft penalty; and (c) solves the resulting problem as a bi-level,

receding-horizon optimization in which an outer resilience-weighted routing layer proposes candidate routes and an inner scenario-based energy-control layer evaluates and selects among them, re-solving the joint problem at every stage as disturbances are realized. The main contributions of this paper are summarized as follows:

- A unified discrete-time, nonlinear, stochastic hybrid state–space model that couples battery energy, SoC, and state-of-health dynamics with vehicle longitudinal dynamics, regenerative braking, charging-station dynamics, and a stochastic infrastructure-uncertainty model.
- A new operational resilience metric is defined on the set of charging station reachability margins from the set of stations reachable from the current state without violating the minimum SoC. Unlike conventional reserve penalties or destination-only feasibility checks, we require nonempty downstream charging reachability as a primary feasibility screen, with the margin penalty serving as a secondary shaping term. In the reported experiments, this requirement is applied as an empirical scenario-based test over S sampled realizations; it is not a certified probabilistic guarantee.
- An approximate mixed discrete-continuous, receding-horizon procedure is proposed in Algorithm 1. The outer layer generates resilience-weighted route candidates, while the inner layer evaluates rather than continuously optimizes their charging controls. Charging power at a visited station is fixed by the resilience-margin threshold rule in Equation (18). The candidate routes are re-evaluated after new traffic, road, or charger information is observed. Accordingly, Equation (23) is the idealized formulation motivating the procedure, not an optimization problem solved exactly in the reported experiments.
- A Monte Carlo performance evaluation on a representative long-distance corridor with a realistic alternate-route topology and charging station siting, benchmarking the proposed framework against two baselines grounded in the EV-routing literature, together with two independent single-parameter sensitivity analyses over charging infrastructure and traffic uncertainty.

The remainder of the paper is organized as follows. Section 2 reviews related work on energy-optimal EV routing, resilience of electrified road networks, and predictive control for EV energy management. Section 3 develops the mathematical model of the resilience-oriented EV cyber-physical system. Section 4 formulates the REM-RA framework, including the resilience metric, the constrained stochastic optimization problem, the bi-level route-adaptation algorithm, and its recursive feasibility property. Section 5 presents the simulation setup, benchmark comparison, and sensitivity analysis. Section 6 concludes the paper and outlines directions for future work.

Algorithm 1: REM-RA—resilience-oriented predictive energy management and route adaptation.

Input: origin n_0, destination n_f, initial state x_0, horizon H, scenario count S, candidate count K, margin trigger τ_S
Output: executed route π^*, executed control sequence $\{u_k^*\}$, state trajectory $\{x_k\}$

1: $k \leftarrow 0$; $x_k \leftarrow x_0$; current $\leftarrow n_0$; unreliable $\leftarrow \varnothing$
2: while current $\neq n_f$ do
3: Estimate infrastructure state $_k$ from observed history (14)
4: Generate K candidate routes $\left\{\pi_k^{(1)}, \ldots, \pi_k^{(K)}\right\}$ from current to n_f via resilience-weighted shortest-path search with edge weight $w(e_{ij})$ (Equation (30)), excluding stations in 'unreliable'

Algorithm 1: *Cont.*

5: for $i = 1, \ldots, K$ do
6: Sample scenario set $\Omega_k = \left\{ w_k^{(1)}, \ldots, w_k^{(S)} \right\} \sim W_k$ (19)
7: for $s = 1, \ldots, S$ do
8: Propagate $x_\tau^{(s)}$ forward along $\pi_k^{(i)}$ using (16); at each visited station node, compute margin S_τ (Equation (18));
if $S_\tau < \tau_S$ or $SOC_\tau < SOC_{min}+$ buffer then charge (10–13)
9: Accumulate stage costs via $l(x_\tau, u_\tau)$ and terminal cost l_f (21)
10: end for
11: Compute expected cost $J^{(i)}$ via Equation (22)
12: end for
13: $\left(\pi_k^*, u_k^*\right) \leftarrow arg\ min_i\ J^{(i)}$ subject to (25)–(28) (Equation (31))
14: Apply first control action u_k^* and routing decision to next node n'
15: Observe realized disturbance w_k; $x_{k+1} \leftarrow f(x_k, u_k*, w_k)$ (16)
16: if a station at n' is realized unavailable, then
17: unreliable $\leftarrow$ unreliable $\cup\{n'\}$
18: end if
19: $k \leftarrow k+1$; current $\leftarrow n'$
20: end while
21: return executed route, executed controls, state trajectory

2. Related Work

Early research on EV routing problems demonstrated that energy consumption cannot be considered as an edge cost to break standard shortest-path algorithms [9]. Regenerative braking adds negative edge costs, and battery capacity limits mean that the cost of a path is greater than the sum of its edge costs. The authors in [4,5] addressed the aforementioned issue by modifying Dijkstra's algorithms, using potential functions and consistency arguments. It is further extended in [6] to determine whether a battery EV can complete the whole trip. The authors in [6] also formalized reachability and connectivity within a short range and allowed for en-route recharging. In [7], the authors removed this simplification by representing the optimal energy consumption relationship between two locations as a continuous function of the initial state of charge (a "profile"). It enabled selection of an economical partial charge rather than a full one, and demonstrated practical, near-real-time computation on large-scale road networks. All these formulations, however, are deterministic and solved once for a static, fully known network. The authors in [1] developed a two-stage traffic-assignment framework to quantify the resilience of an electrified road network subject to random fast-charging station failures. It was shown that station placement and outage duration materially affected system-wide performance.

Model predictive control has become a dominant approach for onboard EV and hybrid EV energy management [10] because it handles multiple time-varying constraints within a receding-horizon loop. The authors in [8] provided a recent systematic review of MPC applications across EV and vehicle-to-grid energy management, documenting consistent gains in efficiency, power quality, and battery lifespan metrics across more than a hundred studies. Ref. [8] is almost exclusively concerned with the continuous power allocation problem for a given route. It rarely couples the energy controller to a discrete online replanned routing decision, which is the gap this paper addresses. To make the

probabilistic resilience requirement of Section 4 tractable, an approach is followed for chance-constrained and robust optimization [11]. This replaced a probabilistic constraint with a finite set of sampled realizations and provided an explicit, distribution-free bound on the probability that the resulting solution violates the original constraint [12]. This technique has been applied to robust control design more broadly [13]. We adopt this scenario-based approximation as the formal basis for the chance constraint used in the constrained stochastic optimization problem of Section 4.5, rather than proposing a new theoretical approximation scheme.

Expanded Literature Review

The recent research between 2020 and 2024 has shown that there is a clear trend from a static or rule-based supervisory control to predictive energy management through learning, route preview, and receding-horizon optimization. For instance, the authors in [14] suggested a multi-neural-network predictive approach for a multi-mode plug-in hybrid EV and reported a 23.40% decrease in computation time, compared to a conventional PMP-based MPC scheme. In [15], the authors integrated driving-profile segmentation with analytical SoC planning and achieved up to 2.09% fuel savings in hilly driving. The authors in [16] introduced electric-motor thermal dynamics with predictive control and highlighted the online applicability by offering a computational-efficiency improvement of four times compared to a DP-based MPC. The authors in [17] then extended their MPC algorithm to incorporate deep reinforcement learning for full EVs in the scenario of car following and road slope, with reported energy savings of 3.2%.

Another line of research shifted from the powertrain level prediction to route-coupled decision-making. The authors in [18] formalized EV routing with public charging stations and explicitly compared rollout logic to a myopic policy, thereby strengthening the case for anticipative route control. The online eco-routing problem was formulated as a combinatorial multi-armed-bandit (MAB) problem in [19] and achieved energy saving of 4.1% compared to shortest-distance routing and 5.4% compared to shortest-trip-time routing. The authors in [20] showed that uncertainty in the available range greatly influences the choice of en-route charging and that ignoring the uncertainty results in overestimation of the charging demand. The results are directly relevant to resilience-oriented predictive management since they demonstrate that the charging demand, the route feasibility, and the decision quality reduce when uncertainty is not included in the control layer.

The most recent research on route adaptation with charger uncertainty is in the areas of charger-state-aware and delay-aware routing. In [21], the authors proposed adaptive EV route planning supported by a charging-station database and reported up to a 97% reduction in average waiting time for EVs, from 6:03 h to 11 min, and also a significant improvement in query resolution. In [22], the authors used charging-station occupancy data for dynamic shortest-path routing and achieved an average reduction in waiting time at the charging stations ranging from 23.7% to 95.4% and an average reduction in the overall trip time of 1.4–18.5%. The authors in [23] showed that charging-station states are important in the structure of the routing objective, as well as highlighting the benefits of using random, minimum-distance, or charging-state-aware routing strategies. In [24], the authors demonstrated that total travel time can be cut by 50% as compared to the state of the art. At the same time, ref. [25] proved the effectiveness of eco-friendly fleet routing in real traffic, with reductions of up to 31% on energy consumption relative to a baseline.

Recent battery EV work also indicates that predictive energy management benefits from hybrid prediction rather than pure first-principles modeling alone. The authors in [26] integrated a physics-based battery EV model with data-driven correction layers. They reduced the average prediction error from 40% for the pure physics model to 10% for the

hybrid model. More recently, ref. [27] used a nationwide analytics-based assessment to link natural hazard and power outage risk indices directly to charging infrastructure exposure. This provides further empirical support, at the network scale, for treating charging station unavailability as a first-class disturbance rather than a rare edge case. Complementarily, ref. [28] developed a robust scenario-based EV charging scheduling formulation under uncertain demand and deadlines, addressing the scenario approximation for scheduling. As a whole, the literature reveals significant advances in predictive control, charging-state awareness, delay-aware replanning, and hybrid energy forecasting. However, the field remains methodologically fragmented: predictive EMS papers still focus mainly on power split or efficiency, whereas routing papers often optimize waiting or trip time without regulating downstream charging reachability as an explicit control variable.

The gap inspired the present manuscript, which focuses on combining predictive energy management, route adaptation, reserve preservation, and uncertainty-aware charging feasibility in a resilience-oriented closed-loop control system. Referring to available literature, REM-RA differs from [4–7] in treating traffic and charging-station availability as stochastic disturbances resolved online rather than as static. It differs from [1] in operating at the level of an individual vehicle's predictive controller rather than system-wide traffic assignment. It also differs from the generic MPC-based EV energy management [8] by coupling the continuous energy-control problem to a discrete, resilience-weighted routing decision that is itself re-optimized at every planning instant. Moreover, it applies the scenario-based machinery of [12,13] to a joint routing and charging decision rather than to a purely continuous control problem. The novelty of the proposed framework is its embedding in this reachability-constrained, mixed discrete-continuous EV control architecture. A summary of the most relevant recent papers and the benchmark comparison metrics that are useful for positioning the proposed REM-RA framework is shown in Table 1.

Table 1. Expanded 2020–2024 literature for predictive, uncertainty-aware, and route-adaptive EV energy management.

Reference	Year	Method Focus	Reported Metric	Benchmark/Comparator
[14]	2020	Predictive multi-neural-network EMS	23.40% lower computation duration	Conventional PMP-based MPC
[15]	2021	Driving-profile segmentation with analytical SoC planning	Up to 2.09% fuel saving; 0.49% max gap to near-global optimum	Traditional approach/near-global optimum
[16]	2022	Predictive EMS with electric-motor thermal dynamics	4× computational-efficiency improvement in accessible summary	DP-based MPC reference
[17]	2022	Learning MPC for FEV eco-driving	3.2% overall energy saving	Baseline control/energy management strategy
[18]	2021	EV routing with public charging stations	Rollout benchmark reported; exact percentage not exposed in accessible summary	Myopic policy
[19]	2022	Online eco-routing under uncertainty	4.1% energy saving vs. SDP; 5.4% vs. STTP	Shortest-distance path and shortest-trip-time path
[20]	2023	Charging-choice modeling under available-range uncertainty	Omitting uncertainty overestimates charging demand	Models ignoring AR uncertainty

Table 1. *Cont.*

Reference	Year	Method Focus	Reported Metric	Benchmark/Comparator
[21]	2022	Adaptive route planning with charging-station database	Up to 97% waiting-time reduction; 6:03 h to 11 min	No-CSDB/lower-penetration baseline
[22]	2024	Occupancy-informed dynamic routing	23.7–95.4% waiting-time reduction; 1.4–18.5% trip-time reduction	Observe charger status only on arrival
[23]	2024	Routing with charging-station states	Comparative framework reported; single percentage not exposed	Random and minimum-distance strategies
[24]	2024	Proactive EV route planning	50% lower total travel time	State-of-the-art route planner
[25]	2024	Eco-friendly routing of EV fleet	Up to 31% lower energy consumption	Baseline routing
[26]	2022	Hybrid predictive energy model for BEVs	Average prediction error reduced from 40% to 10%	Pure physics model
This work	2026	Stochastic reachability-constrained route-energy MPC	99.3% success; 21.5% lower cost; 42% fewer stops	NSD/GFC; unique: probabilistic reachable-charger constraint and online route/control re-optimization

3. Mathematical Modeling of the Resilience-Oriented Electric Vehicle Cyber-Physical System

This section develops the dynamic mathematical model of the resilience-oriented EV cyber-physical system. We first establish the notation used throughout. The transportation network is formulated using graph theory as $G = (N, E)$, consisting of nodes and roads. The graph G represents the road network, where N is a set of intersections and $E = e_{ij} \subseteq N \times N$ represents road segments. The charging stations are represented by $C = \{c_1, c_2, \ldots, c_M\}$, and $T = \{0, 1, \ldots, H\}$ is the prediction horizon. The road-segment length is d_{ij}, and the average road slope is θ_{ij}. The traffic density is ρ_{ij}, and the average velocity is v_{ij}. The travel time is $T_{ij} = d_{ij}/v_{ij}$.

3.1. Battery Dynamic Model

The battery is the main source of energy for EVs and is the most critical subsystem impacting the feasibility of a route and mission resilience. This work models the battery's energy, health, and power states simultaneously, whereas traditional formulations consider the battery's SOC.

3.1.1. Battery Energy Dynamics

Let $E_k \in [0, E_{max}]$ denote the available battery energy at time step k. The battery energy evolves according to

$$E_{k+1} = E_k + \eta_c \cdot P_{c,k} \cdot \Delta t - (P_{tr,k}/\eta_d) \cdot \Delta t + \eta_r \cdot P_{r,k} \cdot \Delta t \quad (1)$$

where $P_{tr,k}$ is traction power demand, $P_{c,k}$ denotes charging power, $P_{r,k}$ denotes regenerative braking power, η_c is charging efficiency, η_d is discharging efficiency, η_r is regenerative

efficiency, and Δt denotes the sampling interval. Equation (1) captures charging, propulsion, and regenerative recovery within a single energy balance.

3.1.2. State-of-Charge Dynamics

The state of charge is defined as $SOC_k = E_k / E_{max}$. Dividing (1) by E_{max} gives

$$SOC_{k+1} = SOC_k + (\Delta t / E_{max}) \cdot (\eta_c \cdot P_c - P_{tr} / \eta_d + \eta_r \cdot P_r) \quad (2)$$

3.1.3. Battery State of Health

Battery state of health degrades under aggressive charging, deep discharge cycling, and thermal stress and evolves on a slower timescale than SOC. Let $SOH \in [0, 1]$; the degradation rate model is

$$SOH_{k+1} = SOH_k - \Delta t \cdot \left(\alpha_1 |P_b| + \alpha_2 (\Delta SOC)^2 + \alpha_3 \cdot T_b \right) \quad (3)$$

where T_b is battery temperature, P_b is battery power, and α_i are experimentally identified degradation coefficients. In the reported experiments, $\alpha_1 = 2.0 \times 10^{-5}$ (SOH loss per kW of $|P_b|$), $\alpha_2 = 0.08$ (SOH loss per unit $(\Delta SOC)^2$), and $\alpha_3 = 1.5 \times 10^{-5}$ (SOH loss per °C), as evaluated with a nominal battery temperature of 32 °C perturbed by zero-mean Gaussian noise (standard deviation 1.5 °C). A full electro-thermal battery model is not implemented, and T_b is therefore a simplifying proxy rather than a simulated thermal state. These coefficients were selected to keep single-trip degradation within the range typically reported for DC fast-charging heavy usage and are not independently calibrated against manufacturer or laboratory cycling data. The Δt scaling makes (3) a proper rate law consistent with (1) and (2), rather than a per-step penalty with inconsistent units.

3.2. Vehicle Longitudinal Dynamics

Vehicle longitudinal motion follows Newton's second law:

$$m \cdot \dot{v} = F_t - F_r - F_d - F_g \quad (4)$$

with rolling resistance $F_r = m \cdot g \cdot C_r$, aerodynamic drag $F_d = 1/2 \cdot \rho \cdot A \cdot C_d \cdot v^2$, road-grade force $F_g = m \cdot g \cdot sin\theta$, and traction force $F_t = P_{tr} / v$. Substituting gives the coupled vehicle-energy relation:

$$m \cdot \dot{v} = P_{tr} / v - m \cdot g \cdot C_r - 1/2 \cdot \rho \cdot A \cdot C_d \cdot v^2 - m \cdot g \cdot sin\theta$$

Discretizing with forward Euler:

$$v_{k+1} = v_k + (\Delta t / m) \cdot \left(P_{tr} / v_k - m \cdot g \cdot C_r - 1/2 \cdot \rho \cdot A \cdot C_d \cdot {v_k}^2 - m \cdot g \cdot sin\theta \right) \quad (5)$$

3.3. Energy Consumption Model

Instantaneous power demand is $P_{tr} = v \cdot \left(F_r + F_d + F_g + m \cdot \dot{v} \right)$. Expanding using (4):

$$P_{tr} = m \cdot g \cdot C_r \cdot v + 1/2 \cdot \rho \cdot A \cdot C_d \cdot v^3 + m \cdot g \cdot v \cdot sin\theta + m \cdot v \cdot \dot{v}. \quad (6)$$

Equation (6) provides a distance-based energy model that captures speed changes, road grade, and aerodynamic losses. The propulsion energy required to traverse a road segment e_{ij} is

$$E_{ij} = \int_{t_i}^{t_j} P_{tr}(t) dt \quad (7)$$

where the integral accounts for varying speed, grade, and traffic conditions along the segment.

3.4. Regenerative Braking Model

Kinetic energy is partially recoverable during deceleration. The recoverable energy is

$$E_{regen} = \eta_r \cdot \left(1/2 \cdot m \cdot \left({v_i}^2 - {v_f}^2\right)\right), v_i > v_f \tag{8}$$

with corresponding regenerative power $P_r = E_{regen}/\Delta t$, which feeds back into (1) and closes the energy loop.

3.5. Vehicle Position Dynamics

Vehicle motion along the transportation network is given by

$$l_{k+1} = l_k + v_k \cdot \Delta t \tag{9}$$

where l_k is the traveled distance along the active route. At graph nodes ($l_k \in N$), the routing decision becomes active.

3.6. Charging Station Model

For charging station j, the charging power is

$$P_{c,k} = \delta_j, k \cdot P_j^{max} \tag{10}$$

where $\delta_j(k) \in \{0,\ 1\}$ indicates whether the EV is connected to station j. The corresponding battery charging dynamics are

$$E_{b,k+1} = E_b, k + \eta_c \cdot P_c, k \cdot \Delta t \tag{11}$$

The charging duration required to reach a target SOC is

$$T_c = \left(\left(SOC_{ref} - SOC\right) \cdot E_{max}\right) / \left(\eta_c \cdot P_c\right) \tag{12}$$

Accounting for congestion, the total charging delay is

$$T_{wait} = T_q + T_c \tag{13}$$

where T_q is the queue waiting time.

3.7. Infrastructure Uncertainty Model

The infrastructure state vector is $I_k = [A_k; Q_k; R_k]$, where A_k is charging availability, Q_k is the queue length, and R_k is road accessibility. Its evolution is modeled as

$$I_{k+1} = f_I(I_k, w_{I,k}) \tag{14}$$

where $w_{I,k}$ represents stochastic disturbances such as charger failures, traffic incidents, or road closures.

3.8. Hybrid State Equation

Combining the battery, vehicle, position, and infrastructure dynamics yields the complete cyber-physical state-space model. The state vector x_k, control vector u_k, and disturbance vector w_k are defined as

$$\begin{aligned} x_k = [SOC_k, SOH_k,\ E_k, v_k, l_k, \pi_k, I_k]^T, \quad u_k = [P_b, P_r, P_c, r_k]^T, \quad w_k \\ = \left[\delta^{traffic},\ \delta^{road}, \delta^{station}, \delta^{weather}\right] \end{aligned} \tag{15}$$

where E_k is the remaining battery energy, v_k is vehicle velocity, l_k is vehicle location, π_k is the active route, and I_k is an infrastructure state. The control input contains battery power P_b, regenerative power P_r, charging power P_c, and routing decision r_k. The disturbance vector represents traffic, road, station, and weather uncertainty. Using (2), (3), (5), (6), (8), (9), and (14), the hybrid discrete-time nonlinear stochastic model is

$$x_{k+1} = f(x_k, u_k, w_k) \tag{16}$$

where $f(\cdot)$ captures the coupled dynamics of battery evolution, vehicle motion, infrastructure interaction, and routing.

4. Resilience-Oriented Predictive Energy Management and Route-Adaptation Framework

Building on the hybrid state–space model in (16), this section formulates the REM-RA problem. The framework couples receding-horizon energy control with discrete routing decisions on the graph $G = (N, E)$, subject to stochastic disturbances arising from traffic, charging-infrastructure availability, and road accessibility.

4.1. Problem Statement

Given an origin node $n_0 \in N$, a destination node $n_f \in N$, and an initial state x_0, the objective is to determine a control sequence $\{u_k\}$, $k = 0, \ldots, H-1$ and an associated route $\pi_k \subseteq G$, such that the vehicle is transported from n_0 to n_f while satisfying the following conditions:

(i) Minimizing energy expenditure, travel time, and battery degradation.
(ii) Maintaining the feasibility of the state trajectory under (16) for all realizations of w_k within a bounded uncertainty set.
(iii) Preserving the capacity to reach a feasible energy replenishment state at every stage, even after disturbance realizations that were not anticipated at the previous planning instant.
(iv) Together, conditions (i) to (iii) distinguish REM-RA from a nominal energy-optimal routing problem: resilience is treated not as a soft penalty but as a state-dependent feasibility requirement, as formalized below.

4.2. Resilience Metric

Define the reachable charging set at the stage k as the set of charging stations the vehicle can reach without violating the minimum state-of-charge bound SOC_{min}:

$$R_k(x_k) = \left\{ cm \in C | SOC_k - (1/E_{max}) \cdot \sum_{e_{ij} \in \pi_{k \to m}} E_{ij} \geq SOC_{min} \right\} \tag{17}$$

where $\pi_{k \to m}$ denotes the shortest feasible path from the vehicle's current position l_k to station c_m, and E_{ij} is computed from (7). The scalar resilience margin is defined as

$$S_k(x_k) = SOC_k - SOC_{min} - max_{c_m \in R_k} (1/E_{max}) \cdot min_{\pi_{k \to m}} \sum_{e_{ij} \in \pi_{k \to m}} E_{ij} \tag{18}$$

The trajectory is called resilient at the stage k if $R_k(x_k) \neq \varnothing$ and $S_k(x_k) \geq 0$. This margin is carried forward as a state-dependent constraint in the predictive controller (Section 4.5), so that the optimizer is explicitly penalized for eroding reachability even when the nominal trajectory remains feasible. If $R_k(x_k) = \varnothing$, then $S_k(x_k) = -1$, and it is registered as a resilience violation by the $max(0, -S_k)$ penalty in (21) and by the feasibility check in (28) and represents the critical failure event. $R_k(x_k)$ is defined in (17) as the energy reachable set, and it identifies the charging stations that can be reached without

violating SOC_{min} under the current energy estimates (independent of whether the stations are currently operational). The real-time station availability is formulated through the routing edge weight in (30). The unavailable stations are removed from consideration in subsequent replanning and excluded from R_k from that point onward.

4.3. Uncertainty Representation

The disturbance vector $w_k = \left[\delta^{traffic}, \delta^{road}, \delta^{station}, \delta^{weather}\right]^{\mathrm{T}}$ introduced in (15) is treated as a random vector with a known or estimated distribution $w_k \sim W_k$. Direct propagation of W_k through the nonlinear map (16) is intractable in closed form, so we approximate the reachable state distribution using a finite scenario set

$$\Omega_k = \{w_k^{(1)}, w_k^{(2)}, \ldots, w_k^{(S)}, w_k^{(s)}\} \sim W_k \tag{19}$$

generated at each planning instant from historical traffic and infrastructure-outage statistics. Each scenario propagates an independent state trajectory

$$x_{k+1}^{(s)} = f\left(x_k, u_k, w_k^{(s)}\right), \quad s = 1, \ldots, S \tag{20}$$

and constraints that must hold in expectation or with high probability are enforced jointly across the scenario set (Section 4.5). This scenario-based treatment, following the scenario approach to chance-constrained and robust optimization [12,13], avoids the conservatism of worst-case robust formulations while retaining a tractable, finite-dimensional optimization problem at each horizon.

4.4. Multi-Objective Cost Functional

The predictive controller minimizes a stage-wise cost that trades off energy cost, travel time, battery degradation, and resilience erosion. The stage cost is

$$l(x_k, u_k) = \lambda_1 \cdot \left(\eta_c{}^{-1} \cdot P_c, k \cdot c_{elec,k}\right) + \lambda_2 \cdot T_{ij}, k + \lambda_3 \cdot |SOH_k - SOH_{k+1}| + \lambda_4 \cdot max(0, -S_k) \tag{21}$$

where $c_{elec,k}$ is the time-varying electricity price at the connected station, and $\lambda_1, \ldots, \lambda_4 \geq 0$ are user-specified weights (energy cost, travel time, degradation, and resilience penalty, respectively). The last term penalizes only the negative resilience margin, so nominal trajectories with $S_k \geq 0$ incur no penalty. The finite-horizon expected cost over the prediction horizon H is

$$J(x_k, u_k) = E_w\left[\Sigma_{\tau=k..k+H-1} l(x_\tau, u_\tau) + l_f(x_{k+H})\right] \approx (1/S) \cdot \Sigma_{s=1\ldots S}\left[\Sigma_{\tau=k\ldots k+H-1} l\left(x_\tau^{(s)}, u_\tau\right) + l_f\left(x_{k+H}^{(s)}\right)\right] \tag{22}$$

with terminal cost $l_f(x_{k+H}) = \lambda_5 \cdot \left(SOC_{ref} - SOC_{k+H}\right)^2$ penalizing deviation of the terminal SOC from the reference required at the destination or next mandatory charging stop.

4.5. Constrained Stochastic Optimization Problem

At each planning instant k, the controller solves

$$min_{u_k = \{u_k, \ldots, u_{k+H-1}\}} \; J(x_k, u_k) \tag{23}$$

subject to, $\forall$ scenarios $s = 1, \ldots, S$ and $\tau \in \{k, \ldots, k+H-1\}$:

$$x_{\tau+1}^{(s)} = f\left(x_\tau^{(s)}, u_\tau, w_\tau^{(s)}\right) \tag{24}$$

$$SOC_{min} \leq SOC_\tau^{(s)} \leq SOC_{max} \tag{25}$$

$$SOH_{\tau}^{(s)} \geq SOH_{min} \tag{26}$$

$$0 \leq P_{c,\tau} \leq P_{j}^{max}, P_{tr,\tau} \leq P_{tr}^{max} \tag{27}$$

$$Pr_{R_{\tau}^{(s)}(x_{\tau}^{(s)})\neq\varnothing} \geq 1-\varepsilon \tag{28}$$

$$r_{\tau} \in N\left(l_{\tau}^{(s)}\right) \tag{29}$$

Constraint (28) is a chance constraint requiring that the reachable charging set defined in (17) remains nonempty with probability of at least $1-\varepsilon$ across the scenario ensemble, which is the mechanism by which resilience is enforced as a hard (probabilistic) requirement rather than only a soft cost term; its numerical approximation follows the sample-complexity results of the scenario approach [12]. The inner-level evaluation uses $S = 12$ sampled scenarios per candidate route, whereas the sample complexity bounds of [12,13] would certify a violation probability ε at confidence $1-\beta$ scale with the number of effective decision variables and require substantially more samples than S = 12 for a decision problem of the same dimension (K = 3 candidate routes, each with continuous power allocation and discrete charging decisions at multiple stations). Constraint (28) is therefore implemented as an empirical, scenario-based resilience heuristic (without a decision confidence calculation) that concentrates evaluation effort on avoiding stranding. Constraint (29) restricts the routing decision r_{τ} at each stage to the outgoing-edge neighborhood $N\left(l_{\tau}^{(s)}\right)$ of the vehicle's current node, coupling the continuous energy-control problem to the discrete graph-search problem.

4.6. Route Adaptation as Bi-Level Re-Optimization

Because π_k enters the cost through the travel-time and energy terms (7) and (21), but is itself a discrete object, (23) is solved as a bi-level problem at each receding-horizon step:

1. Outer level (routing): Given the current infrastructure state estimate $_k$, generate a candidate set of K shortest feasible paths $\left\{\pi_k^{(1)},\ldots,\pi_k^{(K)}\right\}$ from l_k to nf using a resilience-weighted shortest-path search on G, with edge weight

$$w(e_{ij}) = \lambda_1 \cdot \hat{E}_{ij} + \lambda_2 \cdot T_{ij} + \lambda_6 \cdot \left(1 - Pr_{R(e_{ij})\neq\varnothing}\right) \tag{30}$$

penalizing edges whose downstream charging reachability is uncertain.

2. Inner level (energy control): For each candidate route $\pi_k^{(i)}$, the implementation procedure does not solve (23) for the optimal control sequence. Instead, it propagates S samples of disturbance scenarios set with the threshold-triggered charging rule of Algorithm 1. This approximation computes the executed control sequence $u_k^{(i)}$ and the resulting cost $J^{(i)}$.

3. Selection: The executed route and control action are those minimizing $J^{(i)}$ subject to the feasibility of (25)–(28):

$$(\pi_k^*, u_k^*) = arg \ \ min_{i\in\{1,\ldots,K\}} \ \ J^{(i)}\left(x_k, u_k^{(i)}\right) \tag{31}$$

Only the first control action u_k^* and the corresponding next-node routing decision are applied. The candidate set and their scenario evaluations (17) to (31) are recalculated at $k+1$ using updated infrastructure and traffic observations, which is what allows the route to adapt online as $_k$ evolves according to (14).

4.7. Algorithmic Summary

Algorithm 1 summarizes the REM-RA receding-horizon procedure implementing an approximate heuristic solution method for the idealized bi-level problem of Section 4.5

to Section 4.6. At each stage, the vehicle re-evaluates the candidate route set against the currently observed infrastructure state and propagates each candidate over a sampled scenario set. The algorithm selects the resilience-feasible, minimum-expected-cost candidate and executes only the first control and routing action, then repeats after observing the realized disturbance, which is what allows the framework to react to events such as a charging-station outage discovered mid-trip rather than committing irrevocably to a route planned under stale information.

4.8. Conditional Shifted Sequence Feasibility Argument

The shifted sequence construction is only a conditional feasibility argument. It requires the following conditions: (i) the realized disturbance remains within the modelled support, (ii) the shifted controls and appended terminal action remain admissible, (iii) the terminal set $X_f \subseteq X$ that is control invariant satisfies constraints (25) to (27) for the realized state under admitted disturbance, (iv) at least one scenario is feasible, with an available downstream charger or destination state after each update, i.e., the reachable charging set R_k does not become empty due to disturbance realization between planning instants, and (v) no unmodelled outage or closure removes every feasible continuation. These conditions ensure that at stage k, the solution to (23) drives $x_k + H^{(s)} \in X_f$ for all s, then, by construction of (17) to (18), there exists a feasible one-step continuation at $k+1$ that keeps $x_{k+1} + H^{(s)} \in X_f$, obtained by re-applying the tail of the previously optimal input sequence augmented with one admissible action at the new horizon boundary. This standard shifted-sequence argument is stated for the idealized formulation (23) under (28)–(29), and it is a sketch rather than a complete proof. It is not claimed to hold for the approximate procedure of Algorithm 1, whose threshold-based charging rule and finite candidate set do not, in general, return the optimal control sequence that the argument presumes. For the implemented method, the resilience property of Section 4.2 is monitored empirically at every planning instant rather than certified, provided it holds at initialization, i.e., $S_0(x_0) \geq S_{min}$. An event outside (i)–(v) may render the problem infeasible, in which case an emergency fallback policy would be required.

5. Performance Evaluation

This section evaluates the REM-RA framework of Section 4 on a representative long-distance corridor and compares it against two rule-based benchmark strategies based on the EV-routing literature under controlled disturbance conditions. The evaluation covers (i) the simulation environment and case-study network, (ii) vehicle, battery, and infrastructure parameterization, (iii) the stochastic disturbance model used to stress-test the framework, (iv) the benchmark strategies and performance metrics, and (v) Monte Carlo simulation results, including a benchmark comparison and a two independent single parameter sensitivity analysis (including road network disruption and route adaptation). The approximate procedure of Algorithm 1 produces all reported results. The optimization problem (23) is not solved numerically in this section.

5.1. Case-Study Network and Simulation Environment

The framework is evaluated on a 10-node directed graph $G = (N, E)$ representing a 480 km long-distance corridor between Los Angeles and Sacramento, California. The topology reproduces the real alternate-route structure of this corridor: an I-5 direct branch (Bakersfield → Kettleman City → Santa Nella → Manteca) and a CA-99 branch via Fresno (Bakersfield → Fresno → Los Banos → Manteca), which diverge at Bakersfield and reconverge at Manteca before a shared final leg through Stockton to Sacramento. This branching structure is what makes route adaptation (Section 4.6) a useful decision problem, instead

of a trivial single-path problem, since both branches have different lengths, speeds, and spacing of charging stations, and the router is uncertain of all of these factors. Six of the ten nodes (Bakersfield, Kettleman City, Fresno, Santa Nella, Los Banos, Stockton) have DC fast-charging infrastructure, consistent with the approximate real siting of highway DC fast chargers along this corridor. The values of edge distances, free-flow speeds, and road grades used for controlled experimentation are representative values for the corridor and are not as accurate as the GIS data. The value for the free-flow speed for the 1–11 segment in the Grapevine–Bakersfield segment is set at −2.5% descending grade as a result of the Tejon Pass; the term regenerative braking is used (8). Table 2 summarizes the charging-station configuration used in all experiments: rated charging power, energy price, baseline availability probability, and baseline mean queueing delay, all of which parameterize the infrastructure-uncertainty model of (14).

Table 2. Charging-station configuration for the case-study corridor.

Station	Rated Power (kW)	Price ($/kWh)	Baseline Availability	Baseline Queue (min)
Bakersfield	150	0.32	0.97	4
Kettleman City	250	0.34	0.95	6
Fresno	150	0.30	0.96	5
Santa Nella	250	0.35	0.93	8
Los Banos	150	0.31	0.96	5
Stockton	150	0.29	0.97	4

5.2. Vehicle, Battery, and Cost-Weight Parameters

The vehicle and battery parameters in Table 3 are for a typical long-range production EV and remain constant throughout all the experiments. The initial state of charge SOC_0 is not 1.0 but is a realistic value used for a departure, that is, 0.55, in order to have an intermediate charging decision actually needed during the trip of length ≈ 480 km, which lies within the usable battery window $[SOC_{min}, SOC_{max}] = [0.15, 0.95]$; otherwise, the trip is trivially feasible without charging, which would not be used for exercising the routing and charging-decision logic being tested.

Table 3. Vehicle and battery parameters (Equations (1)–(13)).

Parameter	Symbol	Value
Vehicle mass	m	1900 kg
Rolling-resistance coefficient	C_r	0.009
Aerodynamic drag coefficient	C_d	0.24
Frontal area	A	2.4 m^2
Usable battery capacity	E_{max}	75 kWh
Charging efficiency	η_c	0.92
Discharging efficiency	η_d	0.92
Regenerative efficiency	η_r	0.65
Minimum operational SOC	SOC_{min}	0.15
Maximum SOC	SOC_{max}	0.95
Initial SOC	SOC_0	0.55
Target SOC after charging	SOC_{ref}	0.80
Minimum acceptable SOH	SOH_{min}	0.80

The stage-cost weights of (21) and the routing weights of (30) are set to $\lambda_1 = 1.0$ (energy/electricity cost), $\lambda_2 = 8.0$ (travel time), $\lambda_3 = 200$ (battery degradation), $\lambda_4 = 50$ (resilience/stranding penalty), and $\lambda_6 = 40$ (station-reliability penalty in the routing edge weight), chosen so that a single stranding event or sustained negative resilience

margin dominates the expected cost, consistent with resilience being treated as a near-hard constraint rather than a soft preference.

The remaining implementation parameters are as follows. The candidate-route count is $K = 3$. The inner-level scenario count is $S = 12$ (Section 5.6). The chance-constraint violation bound is implemented as $\varepsilon = 0.10$, operationalized as a minimum 90% empirical success rate across the S sampled scenarios for a candidate route to be treated as resilience-feasible in (31). The terminal-cost weight is $\lambda_5 = 0$, i.e., no separate terminal-SOC regularizer is applied in the reported experiments beyond the running resilience penalty λ_4 already present at every stage. This differs from the general formulation in (22) and is stated explicitly here so the results are reproducible as implemented. The outer-level replanning horizon is event-driven rather than a fixed step count: the inner-level evaluation of (22) propagates each candidate route to its terminal node at every replanning instant (i.e., an adaptive H equal to the number of hops remaining to the destination at that instant), while the outer receding-horizon loop re-enumerates and re-evaluates the candidate set after every single hop (Algorithm 1). The decision variables explored at each replanning instant are therefore discrete: the selection among the K = 3 candidate routes, and the threshold-triggered binary charge/no-charge decision at each station visited along a candidate route. Charging power is set by the rated station power and the target SOC of Table 3 and is not optimized as a free continuous variable. The naive shortest-distance benchmark's single-hop reactive charging buffer is 0.05 SOC (five percentage points) above the estimated nominal-condition energy requirement for the next edge. Queueing delay at each station is drawn from a normal distribution with standard deviation equal to 40% of that station's baseline mean queue time (Table 2), truncated at zero. Finally, although the general disturbance vector of (15) includes a weather channel, the numerical experiments of Section 5 instantiate only the traffic and charging-station channels, and the weather channel is not activated in the reported case study. A dedicated road network closure channel is reported in Section 5.7.6.

5.3. Disturbance and Uncertainty Model

Two independent disturbance channels realize w_k in (16) during simulation. (i) A stochastic traffic multiplier is drawn per traversed edge from a truncated normal distribution, $\delta^{traffic} max\left(1, N\left(1 + \sigma_{traffic}, 0.5 \cdot \sigma_{traffic}\right)\right)$, which reduces effective speed and increases congestion-related power losses in (6). (ii) A stochastic charging-infrastructure state realizes I_k in (14) at every visited station; availability is drawn as a Bernoulli trial with probability equal to the station's baseline availability (Table 2), reduced by an outage-boost parameter $\Delta_{station}$, and queueing delay is drawn from a normal distribution centered on the station's baseline queue time. Two operating-point parameters control the overall disturbance severity used throughout the experiments: the traffic-uncertainty magnitude $\sigma_{traffic}$ and the outage-probability boost $\Delta_{station}$. Unless stated otherwise, the benchmark comparison in Section 5.7 uses a moderate-stress operating point of $\sigma_{traffic} = 0.15$ and $\Delta_{station} = 0.15$ (i.e., a 15-percentage-point reduction in station availability relative to baseline).

5.4. Benchmark Strategies

Three routing/energy management policies are compared under identical disturbance realizations.

Proposed (REM-RA): The bi-level resilience-weighted routing and receding-horizon replanning scheme of Section 4.6 and Algorithm 1, with charging decisions triggered by the resilience margin of (18) rather than a fixed SOC threshold, and route re-evaluation triggered whenever a realized disturbance (e.g., a station outage) invalidates the currently assumed

infrastructure state. REM-RA here denotes the implemented approximate procedure of Algorithm 1, not an exact solution of (23).

Naive shortest-distance (NSD): A fixed shortest-distance route computed once and never revised, in the spirit of classical energy-aware EV shortest-path routing [4,5] but without their reachability guarantees. Charging is decided using only single-hop, nominal-condition lookahead; it estimates the energy required for the immediate next edge under undisturbed conditions and charges only if the current SOC would not cover that estimate plus a small, fixed buffer. It has no multi-hop reserve, no resilience margin, and no awareness of traffic or station-outage uncertainty, which is its structural vulnerability.

Greedy full-charge (GFC): The same fixed shortest-distance route as NSD, but charges to SOC_{max} at every station encountered, regardless of need. This reproduces the always-charge-to-full simplification used for en-route recharging in the reachability-based EV routing formulation of [6], a conservative, literature-grounded baseline that trades efficiency for a large safety margin.

Reachability-Aware Threshold (RAT): An ablation baseline RAT uses the same fixed shortest-distance route as NSD and GFC but replaces their charging rules with REM-RA's resilience margin-triggered charging rule (Section 4.2, Equation (18)), while retaining no rerouting capability. Comparing RAT to REM-RA isolates the marginal value of online route adaptation from the marginal value of margin-triggered charging. Comparing RAT to NSD and GFC isolates the marginal value of the charging rule alone.

5.5. Performance Metrics

Eleven metrics are recorded per trial and averaged over the Monte Carlo ensemble: mission success rate (percentage of trials reaching the destination with $SOC \geq SOC_{min}$ throughout); mean travel time, computed over successful trials only; mean energy consumed; mean generalized cost J ((22), including electricity cost, time, degradation, and the resilience/stranding penalty); mean number of charging stops; mean charging-plus-queueing time; mean minimum SOC reached; worst-case (fifth-percentile) minimum SOC, characterizing tail risk rather than the average case; mean battery state of health loss per trip; the resilience-margin violation rate, i.e., the fraction of trials in which $S_k < 0$ (18) at least once; and the mean effective speed.

5.6. Monte Carlo Simulation Protocol

The benchmark comparison uses $N = 150$ independent disturbance realizations per policy at the moderate-stress operating point $\left(\sigma_{traffic} = 0.15, \Delta_{station} = 0.15\right)$. Each sensitivity sweep uses $N = 80$ trials per grid point: a seven-point sweep over $\Delta_{station} \in [0, 0.40]$, a six-point sweep over $\sigma_{traffic} \in [0.05, 0.40]$, and a six-point sweep over the REM-RA resilience-margin trigger threshold. At every planning or replanning instant, the inner level of REM-RA (22) evaluates the expected cost over $S = 12$ scenario realizations per candidate route, following the sample-based scenario approximation of the chance constraint (28) [12,13]. As stated in Sections 4.5 and 4.7, this screening is empirical and uncertified: S = 12 does not satisfy the sample-complexity bounds of [12,13] for a decision problem of this dimension, and no violation probability or confidence level is claimed for it. All experiments use fixed random seeds for reproducibility.

5.7. Results

5.7.1. Representative Trajectory: Routing and Control Actions

Figure 1 shows a representative disturbance realization in which REM-RA selects the I-5 branch (Los Angeles → Grapevine → Bakersfield → Kettleman City → Santa Nella → Manteca → Stockton → Sacramento) over the CA-99 alternative. Two charging control

actions $u_k = P_{c,k}$ are triggered en route, at Bakersfield and at Stockton, each replacing SOC from approximately 40 to 45% to the target $SOC_{ref} = 80$. At Santa Nella, the station is realized to be unavailable (14), and the receding-horizon replanning logic of Section 4.6 registers this and proceeds without charging there, since the resilience margin (18) at that point still certifies Manteca/Stockton as reachable. Figure 2 shows the corresponding SOC trajectory against cumulative distance: both charging events are triggered while a comfortable margin above $SOC_{min} = 15$ remains, and the SOC never approaches the operational floor despite the mid-route station outage, illustrating the intended behavior of the resilience margin-driven charging rule. It does not demonstrate or certify reachability under all disturbance realizations.

Figure 1 shows one representative disturbance realization in which REM-RA selects the I-5 branch. Two charging actions are triggered, at Bakersfield and Stockton. At Santa Nella, the station is realized to be unavailable, and the replanning logic registers the outage and proceeds without charging because, under the current model estimates, the resilience margin indicates that Manteca or Stockton remain reachable. Figure 2 shows the corresponding SOC trajectory. In this particular realization, both charging events occur before the SOC approaches the operational floor. The figure illustrates the intended behavior of the margin-driven rule; it does not demonstrate or certify reachability under all disturbance realizations.

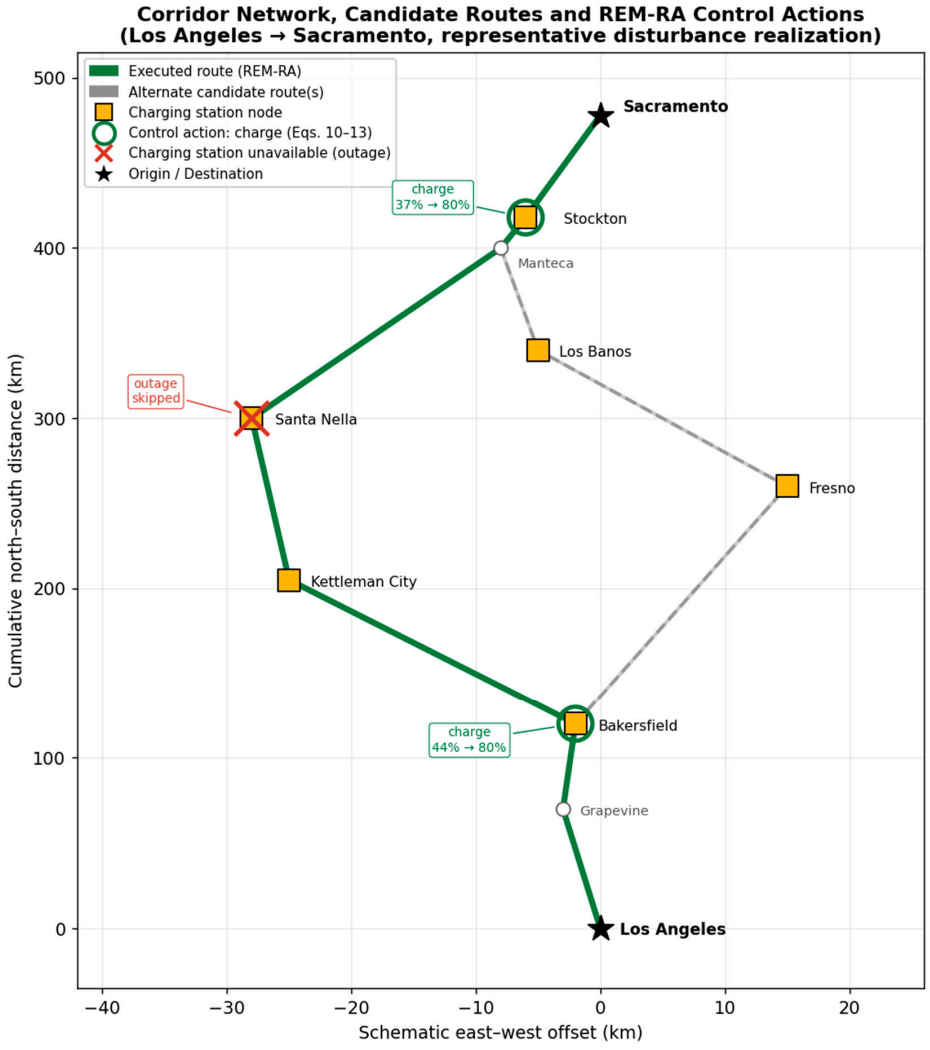


Figure 1. Corridor network with candidate routes, the REM-RA executed route, and control actions (charging events and an outage-driven skip) for a representative disturbance realization.

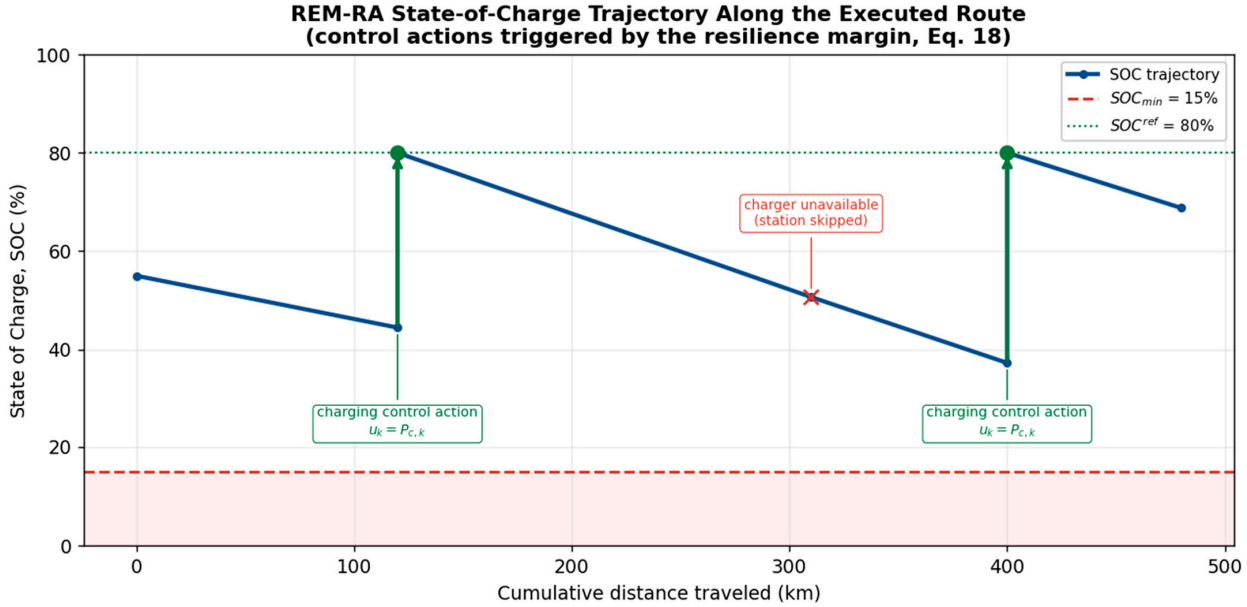


Figure 2. SOC trajectory along the executed route, with control actions annotated at the distance where they occur, relative to the SOC_{min} operational floor and SOC_{ref} charging target.

5.7.2. Benchmark Comparison

Table 4 and Figure 3 report the full Monte Carlo comparison at the moderate-stress operating point. REM-RA and GFC achieve statistically similar mission success (99.3% for both). In comparison, NSD reaches only 67.3%, confirming that single-hop, disturbance-unaware charging is materially unsafe under realistic traffic and infrastructure uncertainty, even though its underlying route is computed with the same shortest-path principle used in classical EV routing [4,5]. Critically, REM-RA achieves this reliability at substantially lower cost than GFC, a mean generalized cost of 20.4 versus 26.0, a 21.5% reduction, while requiring 42% fewer charging stops (1.8 versus 3.1) and 30% less charging-plus-queueing time (0.49 h versus 0.71 h). This is the central result: GFC's reliability comes from over-provisioning charge at every opportunity, in the manner of always charging to the full assumption of [6], whereas REM-RA obtains comparable reliability by charging only when the resilience margin indicates. NSD's mean cost (92.3) is dominated by the stranding penalty incurred in the 32.7% of trials that fail to reach the destination.

Table 4. Benchmark comparison over $N = 150$ Monte Carlo trials per policy at the moderate-stress operating point ($\sigma_{traffic} = 0.15, \Delta_{station} = 0.15$).

Metric	REM-RA	NSD	GFC
Mission success rate (%)	99.3	67.3	99.3
Mean travel time, reached trials (h)	5.91	5.58	5.96
Mean energy consumed (kWh)	53.69	49.49	53.07
Mean generalized cost J	20.43	92.30	26.02
Mean number of charging stops	1.80	1.60	3.10
Mean charging + queue time (h)	0.49	0.28	0.71
Mean minimum SOC reached	0.359	0.182	0.401
Worst-case (5th pct.) minimum SOC	0.180	0.083	0.278
Mean SOH degradation per trip	0.011	0.010	0.010
Resilience-margin violation rate (%)	5.3	4.7	0.0
Mean effective speed (km/h)	81.6	86.1	80.5

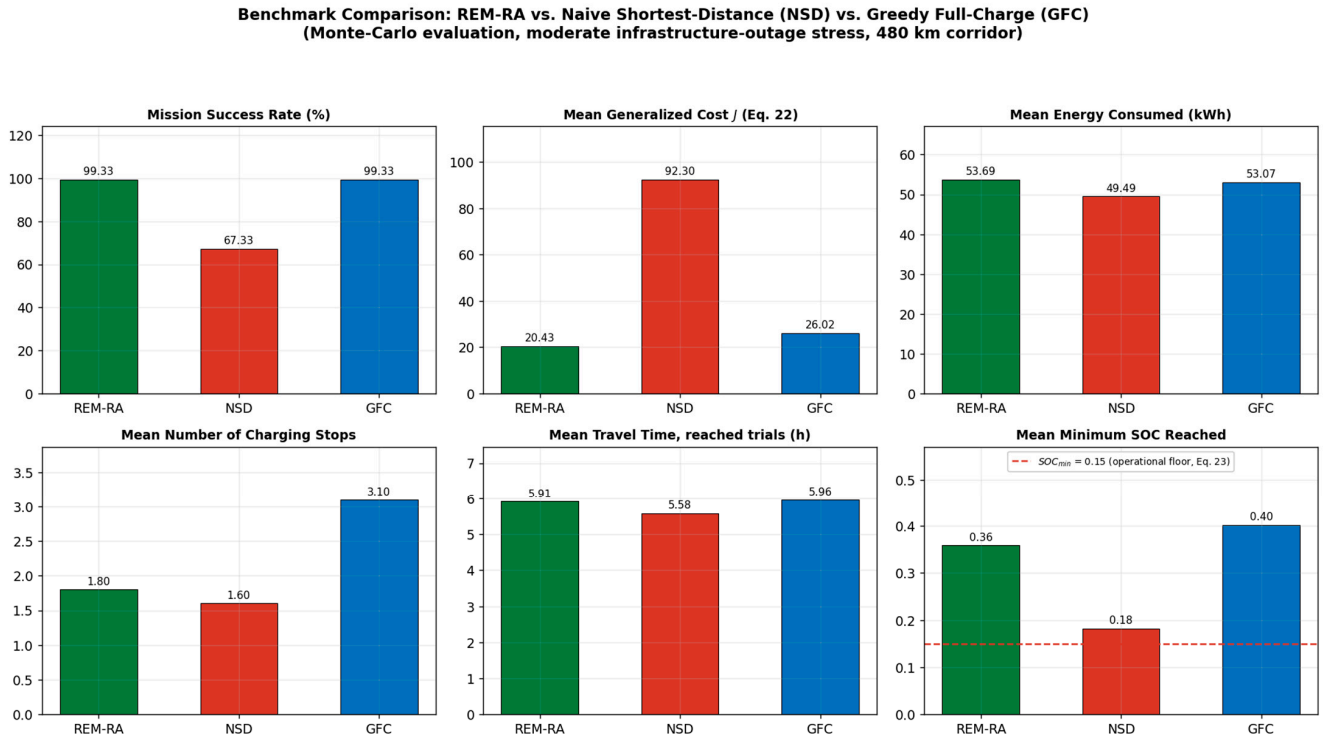


Figure 3. Multi-panel Monte Carlo comparison of REM-RA, NSD, and GFC across six performance metrics, NSD: Naive shortest-distance, GFC: Greedy full-charge.

The worst-case (fifth-percentile) minimum SOC further separates the policies on tail risk: REM-RA sustains 0.180 at the fifth percentile versus 0.083 for NSD. This indicates that even in its worst-case trials, REM-RA remains comfortably clear of the 0.15 operational floor, while NSD's worst-case trials sit essentially on the boundary. The resilience-margin violation rate (fraction of trials in which $S_k < 0$ at least once) is 5.3% for REM-RA versus 4.7% for NSD, which at first appears counterintuitive given NSD's far lower success rate. The explanation is that NSD's failures are concentrated in a single overcommitted leg early in the trip; the simulation terminates on stranding before accumulating further margin checks. In comparison, REM-RA completes the full route in nearly all trials and therefore has more opportunities to register a transient negative margin that it subsequently recovers from by charging. This confirms that the margin-violation indicator should be read alongside success rate and worst-case SOC rather than in isolation. Energy consumption (49.5 to 53.7 kWh), travel time (5.6 to 6.0 h), and battery degradation (≈0.010 to 0.011 SOH loss per trip) are comparable across all three policies, since all follow similar physical routes. The differentiation is driven by charging and routing decisions, not by the underlying vehicle dynamics.

5.7.3. Sensitivity to Charging-Infrastructure Reliability

Figure 4 sweeps the station outage-probability boost $\Delta_{station}$ from 0 to 0.40 while holding $\sigma_{traffic} = 0.15$. At the baseline reliability level ($\Delta_{station} = 0$), all three policies succeed in at least 93.8% of trials; as infrastructure degrades, REM-RA and GFC remain close, with success rates of 91.3% and 88.8%, respectively, at $\Delta_{station} = 0.40$, while NSD collapses from 93.8% to 40.0% over the same range. The cost curves separate far more sharply: NSD's mean cost rises from 28.2 to 158.8 (a 5.6× increase) as repeated near-failures and outright stranding accumulate penalty, whereas REM-RA's cost rises more moderately from 22.3 to 40.3 (1.8×) and remains the lowest of the three policies across the entire sweep. The GFC's costs rise from 25.4 to 49.0 (1.9×). REM-RA therefore degrades gracefully under increasing infrastructure unreliability, consistent with the receding-horizon replanning

mechanism (Section 4.6), adapting the route and charging plan as outages are observed, rather than committing to a single a priori plan. The network-level resilience finding of [1] that station failures materially affect corridor performance is thus mirrored at the single-vehicle level here.

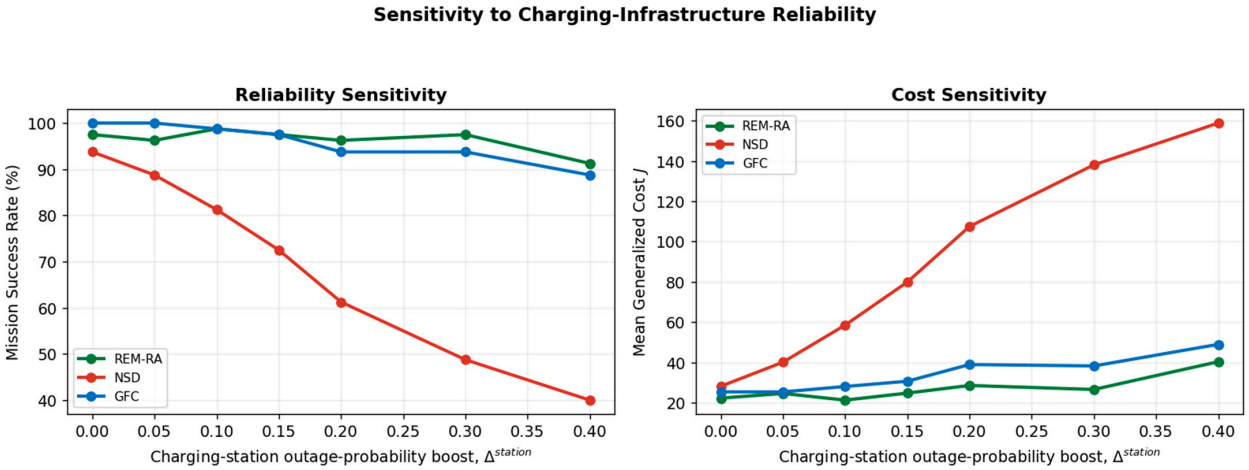


Figure 4. Sensitivity of mission success rate and mean generalized cost to charging-station outage probability ($\Delta_{station}$), all three policies, $N = 80$ trials per point.

5.7.4. Sensitivity to Traffic-Demand Uncertainty

Figure 5 sweeps the traffic-uncertainty magnitude $\sigma_{traffic}$ from 0.05 to 0.40 while holding $\Delta_{station} = 0.15$. REM-RA and GFC both maintain success rates between 95.0% and 98.8% across the full range. In comparison, NSD fluctuates between 67.5% and 78.8%, consistently well below the other two policies, regardless of traffic-uncertainty severity. REM-RA's mean cost is lowest at every sweep point, ranging from 20.1 to 31.8 and generally decreasing at higher $\sigma_{traffic}$ once $\sigma_{traffic} \geq 0.30$. This reflects that a higher traffic multiplier lengthens travel time roughly uniformly across all edges without materially increasing failure risk once the resilience margin has already been calibrated for moderate outage stress, so the dominant cost driver remains the electricity and time terms rather than the stranding penalty. Overall, mission reliability in this corridor is governed primarily by charging-infrastructure availability rather than by traffic-speed variability, which mainly affects travel time and energy consumption rather than the feasibility of the trip.

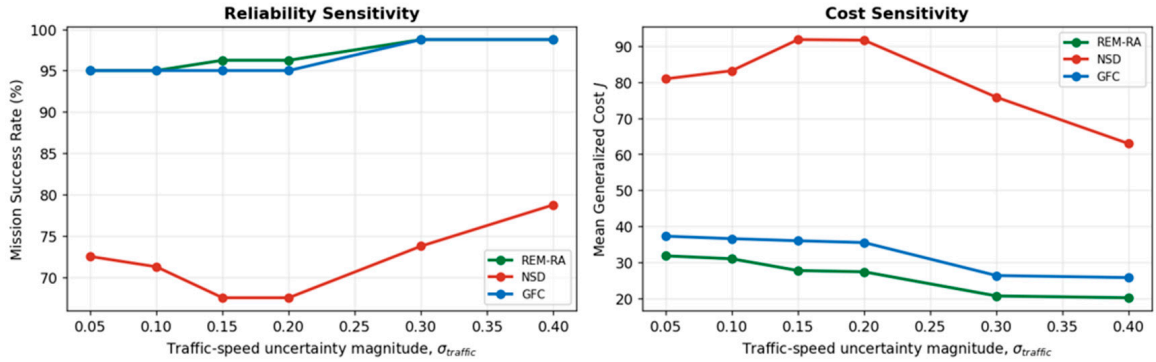


Figure 5. Sensitivity of mission success rate and mean generalized cost to traffic-speed uncertainty magnitude ($\sigma_{traffic}$), all three policies, $N = 80$ trials per point.

5.7.5. Resilience–Cost Trade-Off

Figure 6 isolates the effect of the resilience-margin trigger threshold used in REM-RA's charging decision rule (Section 4.2, Equation (18)) by sweeping its base value from 0.02

to 0.40 at the moderate-stress operating point. At a near-zero threshold (0.02), REM-RA behaves almost reactively, charging only when the margin is already close to exhausted. This yields the highest mean cost (65.3) and the lowest success rate (80.0%) of the sweep, since the vehicle frequently commits to legs it can only marginally complete. Increasing the threshold to 0.15 sharply improves both success rate (93.8%) and cost (33.8, the sweep minimum), as charging is triggered with enough lead time to avoid marginal legs without materially over-provisioning charge. Beyond a threshold of roughly 0.15 to 0.22, both success rate and mean minimum SOC plateau (93.8% success, minimum SOC $\approx$ 0.37), while mean cost begins to rise again (35.8 to 35.9 at thresholds of 0.30 to 0.40) as the policy starts to charge earlier and more often than strictly necessary, converging toward GFC-like over-provisioning. This trade-off curve identifies an operating region around a 0.15 margin-trigger threshold as a favorable balance between reliability and cost for this corridor and disturbance regime. It demonstrates that the resilience-margin threshold is a meaningful, tunable design parameter rather than an arbitrary constant.

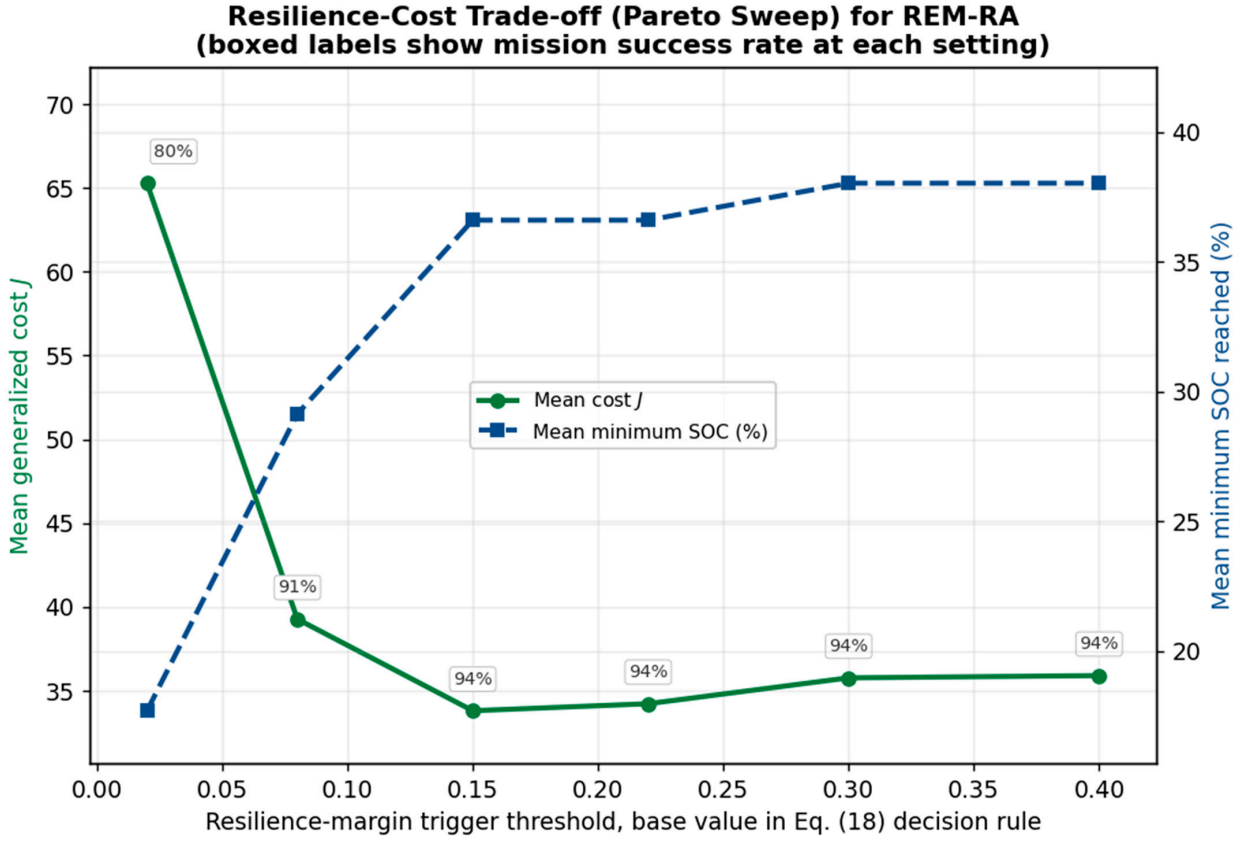


Figure 6. Resilience–cost trade-off for REM-RA as a function of the resilience-margin trigger threshold; point labels report the corresponding mission success rate, $N = 80$ trials per point.

5.7.6. Sensitivity to Road Network Disruption

Road network disruption is analyzed using each directed road segment e_{ij} independently becoming impassable with probability p^{road}. It is realized once per trial and revealed to the vehicle only when it is about to be traversed (i.e., no prior knowledge). REM-RA's receding-horizon replanning (Algorithm 1) excludes a discovered closure from the candidate-route graph and re-solves (30)–(31) from the current node. The three fixed-route benchmarks (NSD, GFC, and the RAT) cannot reroute and register a failed trip (blocked) if a closure falls on their pre-computed path. Figure 7 sweeps p^{road} from 0 to 0.20 at the moderate-stress operating point $\left(\sigma_{traffic} = 0.15,\ \Delta_{station} = 0.15\right)$, $N = 80$ trials per point. At $p^{road} = 0$, results are consistent with Table 4 (REM-RA and GFC near parity, both well

above NSD). As p^{road} increases, REM-RA's advantage over both fixed-route policies widens substantially: at $p^{road} = 0.10$, REM-RA reaches 58.8% success versus 45.0% (GFC) and 31.2% (NSD); at $p^{road} = 0.20$, REM-RA reaches 18.8% versus 11.2% (GFC) and 10.0% (NSD). Mean generalized cost shows the same pattern in reverse: REM-RA's cost grows from 22.6 to 205.4 across the sweep, while NSD's and GFC's costs grow faster, from 79.5/29.5 to 358.7/362.4, respectively, since a blocked fixed route contributes the full stranding penalty with no opportunity to recover via a detour. This experiment identified that charging-rule improvement dominates under a charging-infrastructure-only disturbance.

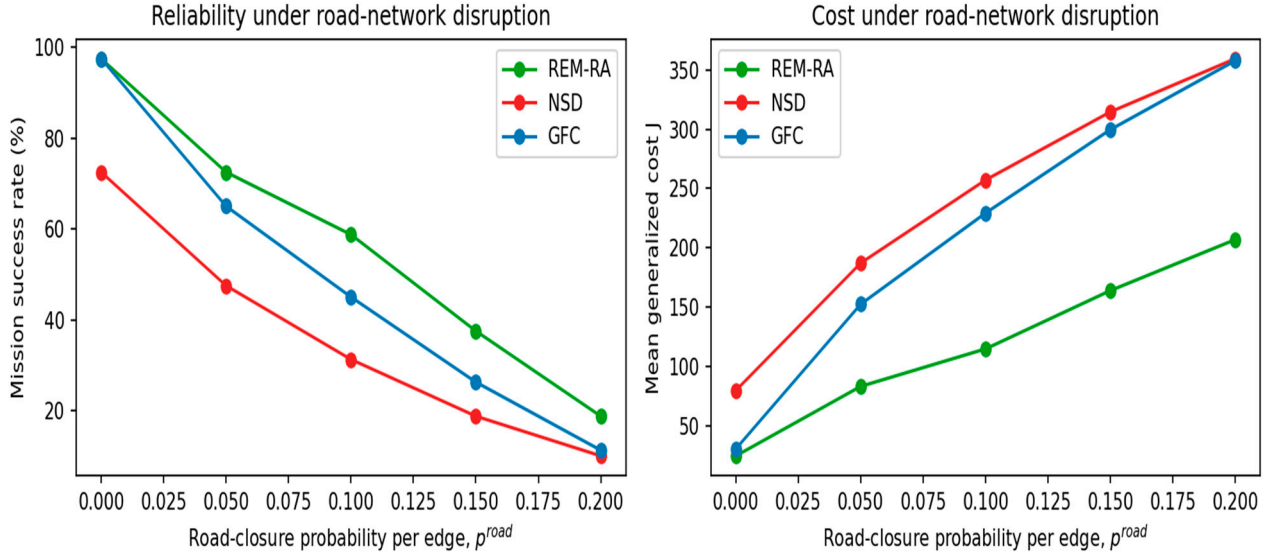


Figure 7. Sensitivity of mission success rate and mean generalized cost to road-closure probability per edge, REM-RA vs. NSD vs. GFC, N = 80 trials per point.

5.7.7. Route-Adaptation Analysis

The benchmark strategies NSD and GFC differ from REM-RA in both their charging rule and their inability to reroute; the comparisons in Table 4 alone cannot attribute REM-RA's advantage to either mechanism individually. We therefore add a fourth policy, a reachability-aware threshold (RAT), which is the same fixed shortest-distance route as NSD and GFC, but using REM-RA's resilience margin-triggered charging rule (Section 4.2, Equation (18)) instead of NSD's single-hop reactive rule or GFC's always-fill rule, and with no rerouting capability. RAT isolates the charging rule improvement from the route adaptation improvement as shown in Figure 8. At the moderate-stress operating point ($N = 150$ trials), RAT achieves 99.3% mission success (95% Wilson CI [96.3, 99.9]) at a mean generalized cost of 20.6 (95% CI [17.5, 23.7]), statistically indistinguishable from full REM-RA (99.3%, CI [96.3, 99.9]; cost 20.4, CI [17.3, 23.6]) and from GFC's success rate, while matching REM-RA's cost far more closely than GFC's (26.0, CI [23.0, 29.0]). This is substantive and useful under the charging infrastructure and traffic-only disturbance regime of Table 4; essentially all of REM-RA's advantage over NSD, and its cost advantage over GFC, is attributable to the resilience-margin charging rule rather than to online route replanning. Route adaptation's distinct marginal contribution becomes material only once road network disruption is introduced (Section 5.7.6), where RAT is unable to reroute around a closure, and it degrades in line with NSD and GFC rather than with REM-RA (RAT is omitted from Figure 7 since it shares GFC's and NSD's fixed route).

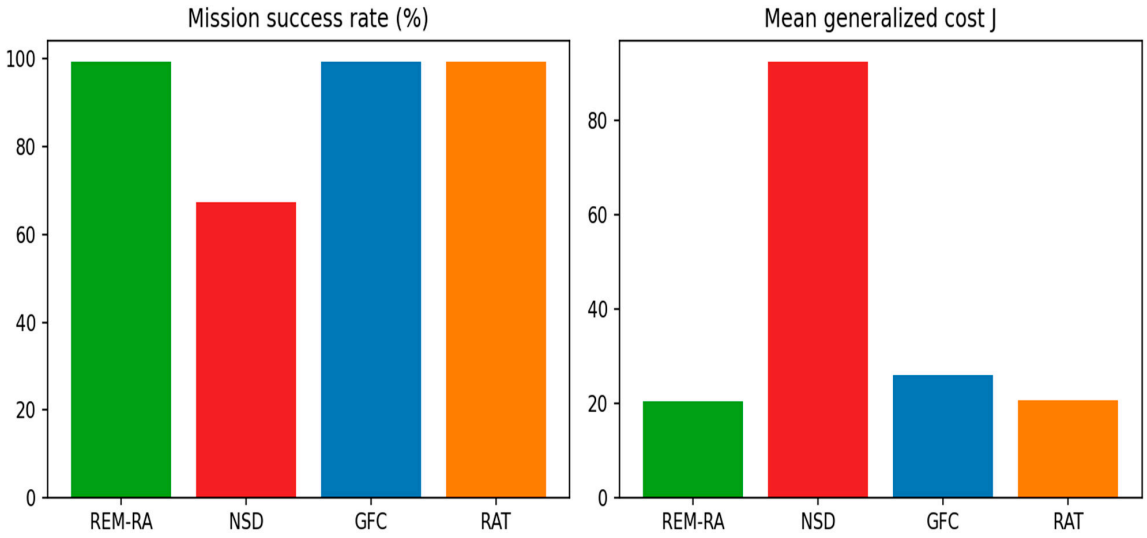


Figure 8. Simulation comparison: REM-RA vs. RAT (fixed route + resilience-margin charging) vs. NSD vs. GFC, N = 150 trials, moderate-stress operating point.

5.7.8. Statistical Interval, Cost Weight Sensitivity, and Computational Runtime Analysis

First, the statistical interval analysis is conducted using 95% confidence intervals for Table 4 (Wilson score intervals for success rate proportions and normal approximation intervals for continuous metrics, both computed from the same N = 150 trial sets). REM-RA's and GFC's success rate intervals are identical to one decimal ([96.3, 99.9] for both, reflecting 149/150 successes each), which is the quantitative basis for the "statistically similar" characterization used in Section 5.7.2. Second, we report a representative cost-weight sensitivity check on λ_4 (the stranding penalty weight), the weight identified in Section 5.2 dominating the objective by design. Sweeping $\lambda_4 \in \{10, 25, 50, 100, 200\}$ at the moderate-stress operating point leaves REM-RA's success rate essentially unchanged (95.0–96.2%) and always well above NSD's (76.2%, unchanged since λ_4, does not affect NSD's rule-based charging logic), while REM-RA's cost advantage over NSD widens monotonically with λ_4 (from a 1.1× to a 4.4× ratio). The qualitative ranking of the two policies is therefore robust to this weight over a 20× range, though the magnitude of the reported cost reduction is a function of the chosen weights. Third, addressing the computational feasibility is analyzed by measuring REM-RA's per-replanning-step time ($K = 3$ candidate routes, $S = 12$ scenarios, each without parallelization) over 150 replanning calls, giving a mean of 22.6 ms, median 24.3 ms, 95th percentile 36.2 ms, and maximum 51.5 ms. These times are one to two orders of magnitude below the multi-minute intervals between highway decision points on this corridor, indicating ample computational headroom for online implementation of the approximate procedure.

5.8. Discussion

Three observations emerge consistently across all experiments. First, resilience-margin-driven charging (REM-RA) reproduces the reliability of a conservative, over-provisioning policy (GFC, in the spirit of [6]) without its efficiency cost, cutting mean generalized cost by roughly a fifth and charging stops by more than two-fifths under moderate stress. Second, ignoring resilience and disturbance uncertainty in the charging decision (NSD, built on classical energy-aware shortest-path routing [4,5]) is not merely inefficient but structurally unsafe: its success rate degrades sharply, and its cost grows super-linearly as either charging-infrastructure reliability or traffic uncertainty worsens, since a single mis-planned leg is often unrecoverable without route replanning. Third, mission reliability on this corridor is more sensitive to charging-infrastructure availability than to traffic-speed uncertainty,

which is consistent with network-level resilience findings for electrified road networks under charging-station failure [1]. This has implications for where resilience-oriented planning provides the greatest operational value: corridors with sparse or unreliable charging infrastructure stand to benefit most from the receding-horizon, margin-aware approach developed in Section 4. The resilience–cost trade-off analysis further shows that the margin-trigger threshold is not a free parameter to be set arbitrarily conservatively: excessively low thresholds erode reliability, while excessively high thresholds erode the efficiency advantage that motivates the framework, confirming the practical relevance of treating the resilience margin as a tunable design parameter rather than a fixed safety factor.

6. Conclusions

This paper proposed a REM-RA framework for long-distance EVs operating under charging infrastructure and road network uncertainty. The framework rests on three elements: (i) a hybrid cyber-physical state-space model coupling battery energy, health, and vehicle longitudinal dynamics with a stochastic infrastructure state (Section 3); (ii) a resilience margin defined on the set of charging stations reachable from the current state, screened by an empirical, uncertified scenario-based feasibility test that approximates the idealized chance constraint, within a bi-level, receding-horizon scheme controller that jointly adapts routing and charging decisions (Section 4); and (iii) a Monte Carlo evaluation on a realistic long-distance corridor with literature-grounded benchmarks (Section 5). The evaluation showed that REM-RA matches the mission-success reliability of a conservative, always-charge-to-full baseline [6] (99.3% vs. 99.3%) while reducing mean generalized cost by 21.5% and charging stops by 42%, and that it substantially outperforms a naive, disturbance-unaware shortest-path baseline built on classical EV routing principles [4,5] (99.3% vs. 67.3% success). Sensitivity analysis further showed that REM-RA degrades gracefully as charging-infrastructure reliability worsens. Section 5.7.7 shows that under charging infrastructure and traffic disturbance alone, the advantage is attributable to the resilience margin charging rule rather than to online route replanning. A road closure sensitivity analysis shows that route replanning's distinct contribution becomes substantial once road network accessibility, rather than only charging-station availability, is uncertain. REM-RA's success rate advantage over both fixed-route baselines widens from near parity to roughly 2x as road-closure probability increases to 0.20. The mission's reliability on the studied corridor is governed primarily by charging-station availability rather than by traffic-speed uncertainty, echoing network-level resilience findings for electrified road networks [1].

Several limitations exist for the proposed study. All the case-study corridor parameters, distances, and disturbance parameters are not empirically calibrated but are representative. The specific numeric outcomes (e.g., the 67.3% NSD success rate, or the favorable region identified in the resilience–cost trade-off) are therefore artifacts of these modeling choices. Re-derivation is required if used in a different corridor or vehicle. The scenario-sampling approximation to chance constraint (28) is not certified in the experiments reported here, since no explicit sample-complexity bound is established for S = 12. Moreover, the results are obtained with the approximate procedure of Algorithm 1 rather than by solving (23), so the reported costs are upper bounds on what an exact solution of (23) could attain; the recursive feasibility argument of Section 4.8 is formulated as a shifted-sequence sketch and not as a complete Lyapunov-based proof with an explicit invariant-set construction. Future research will involve calibration of the disturbance model with the actual availability of public fast chargers and the availability of vehicles on highways, and modeling development from a single vehicle to coordinating multiple vehicles' charging decisions, considering shared station capacity. Formulating the chance constraint (28) explicitly af-

ter the scenario approach in [12,13] and replacing the historical-statistics-driven scenario generation employed here with learned data-driven disturbance forecasts and formally establishing the sample complexity bound, it is necessary to certify the constraint in (28) at a stated confidence level, which are also identified as concrete next steps.

Author Contributions: Conceptualization, B.K. and Z.U.; methodology, B.K. and S.H.; software, B.K.; validation, Z.U. and G.G.; formal analysis, Z.U. and S.H.; investigation, G.G.; resources, G.G.; data curation, S.H.; writing—original draft preparation, B.K. and Z.U.; writing—review and editing, G.G. and S.H.; visualization, Z.U. and S.H.; supervision, B.K.; project administration, G.G. All authors have read and agreed to the published version of the manuscript.

Funding: This research received no external funding.

Data Availability Statement: The original contributions presented in this study are included in the article. Further inquiries can be directed to the corresponding author.

Acknowledgments: This work was supported by the internal project (INSE2628) at the Interdisciplinary Research Center for Sustainable Energy Systems (IRC-SES), King Fahd University of Petroleum and Minerals (KFUPM), Dhahran, Saudi Arabia.

Conflicts of Interest: The authors declare that they have no conflicts of interest.

Nomenclature

Symbol	Definition
$G = (N, E)$	Road network graph; nodes N (intersections) and edges E (road segments)
$C = \{c_1, \ldots, c_M\}$	Set of charging stations
$d_{ij}, \theta_{ij}, \rho_{ij}, v_{ij}$	Length, grade, traffic density, and average speed of edge e_ij
E_k, SOC_k, SOH_k	Battery energy, state of charge, and state of health at step k
P_{tr}, P_c, P_r, P_b	Traction, charging, regenerative, and net battery power
η_c, η_d, η_r	Charging, discharging, and regenerative efficiencies
m, C_r, C_d, A	Vehicle mass, rolling-resistance coefficient, drag coefficient, frontal area
l_k, π_k, I_k	Vehicle position, active route, and infrastructure state at step k
x_k, u_k, w_k	Hybrid system state, control input, and disturbance vectors
$R_k(x_k), S_k(x_k)$	Reachable charging set and scalar resilience margin at step k
Ω_k, S	Scenario set and scenario count used in expected-cost evaluation
$J, l(\cdot), l_f(\cdot)$	Expected cost, stage cost, and terminal cost
$\lambda_1, \ldots, \lambda_6$	Cost- and routing-weight coefficients
ε	Chance-constraint violation probability bound
K	Number of candidate routes evaluated per replanning instant
H	Prediction horizon

References

1. Wang, H.; Abdin, A.F.; Fang, Y.-P.; Zio, E. Resilience assessment of electrified road networks subject to charging station failures. *Comput.-Aided Civ. Infrastruct. Eng.* **2022**, *37*, 300–316. [CrossRef]
2. Khan, B.; Ullah, Z.; Gruosso, G. Enhancing grid stability through physics-informed machine learning integrated-model predictive control for electric vehicle disturbance management. *World Electr. Veh. J.* **2025**, *16*, 292. [CrossRef]
3. Khan, B.; Ali, S.M.; Ullah, Z. Deep learning based digital twins augmented reality: Model predictive control for battery and storage optimization in renewable energy prosumers districts. *J. Energy Storage* **2025**, *131*, 117565. [CrossRef]
4. Andreas, A.; Haselmayr, J.; Leucker, M.; Sachenbacher, M. The shortest path problem revisited: Optimal routing for electric vehicles. In *Annual Conference on Artificial Intelligence*; Springer: Berlin/Heidelberg, Germany, 2010; pp. 309–316.
5. Martin, S.; Leucker, M.; Artmeier, A.; Haselmayr, J. Efficient energy-optimal routing for electric vehicles. *Proc. AAAI Conf. Artif. Intell.* **2011**, *25*, 1402–1407. [CrossRef]
6. Storandt, S.; Funke, S. Cruising with a battery-powered vehicle and not getting stranded. *Proc. AAAI Conf. Artif. Intell.* **2012**, *26*, 1628–1634. [CrossRef]

7. Baum, M.; Dibbelt, J.; Pajor, T.; Sauer, J.; Wagner, D.; Zündorf, T. Energy-optimal routes for battery electric vehicles. *Algorithmica* **2020**, *82*, 1490–1546. [CrossRef]
8. Minchala-Ávila, C.; Arévalo, P.; Ochoa-Correa, D. A systematic review of model predictive control for robust and efficient energy management in electric vehicle integration and V2G applications. *Modelling* **2025**, *6*, 20. [CrossRef]
9. Liu, J.; Lin, G.; Huang, S.; Zhou, Y.; Rehtanz, C.; Li, Y. Collaborative EV routing and charging scheduling with power distribution and traffic networks interaction. *IEEE Trans. Power Syst.* **2022**, *37*, 3923–3936. [CrossRef]
10. Veerendra, A.S.; Bin Mohamed, M.R.; Márquez, F.P.G. Energy management control strategies for energy storage systems of hybrid electric vehicle: A review. *Energy Storage* **2024**, *6*, e573. [CrossRef]
11. Gu, N.; Wang, H.; Zhang, J.; Wu, C. Bridging chance-constrained and robust optimization in an emission-aware economic dispatch with energy storage. *IEEE Trans. Power Syst.* **2021**, *37*, 1078–1090. [CrossRef]
12. Campi, M.C.; Garatti, S. The exact feasibility of randomized solutions of uncertain convex programs. *SIAM J. Optim.* **2008**, *19*, 1211–1230. [CrossRef]
13. Calafiore, G.; Campi, M. The scenario approach to robust control design. *IEEE Trans. Autom. Control* **2006**, *51*, 742–753. [CrossRef]
14. Wu, Y.; Zhang, Y.; Li, G.; Shen, J.; Chen, Z.; Liu, Y. A predictive energy management strategy for multi-mode plug-in hybrid electric vehicles based on multi neural networks. *Energy* **2020**, *208*, 118366. [CrossRef]
15. Zhou, W.; Chen, Y.; Zhai, H.; Zhang, W. Predictive energy management for a plug-in hybrid electric vehicle using driving profile segmentation and energy-based analytical SoC planning. *Energy* **2021**, *220*, 119700. [CrossRef]
16. Han, J.; Shu, H.; Tang, X.; Lin, X.; Liu, C.; Hu, X. Predictive energy management for plug-in hybrid electric vehicles considering electric motor thermal dynamics. *Energy Convers. Manag.* **2022**, *251*, 115022. [CrossRef]
17. Yeom, K. Learning model predictive control for efficient energy management of electric vehicles under car following and road slopes. *Energy Rep.* **2022**, *8*, 599–604. [CrossRef]
18. Kullman, N.; Goodson, J.; Mendoza, J.E. Electric vehicle routing with public charging stations. *Transp. Sci.* **2021**, *55*, 637–659. [CrossRef]
19. Chen, X.; Xue, J.; Lei, Z.; Qian, X.; Ukkusuri, S.V. Online eco-routing for electric vehicles using combinatorial multi-armed bandit with estimated covariance. *Transp. Res. Part D Transp. Environ.* **2022**, *111*, 103447. [CrossRef]
20. Li, H.; Yu, L.; Chen, Y.; Tu, H.; Zhang, J. Uncertainty of available range in explaining the charging choice behavior of BEV users. *Transp. Res. Part A Policy Pract.* **2023**, *170*, 103624. [CrossRef]
21. Schoenberg, S.; Dressler, F. Reducing waiting times at charging stations with adaptive electric vehicle route planning. *IEEE Trans. Intell. Veh.* **2022**, *8*, 95–107. [CrossRef]
22. Dastpak, M.; Errico, F.; Jabali, O.; Malucelli, F. Dynamic routing for the electric vehicle shortest path problem with charging station occupancy information. *Transp. Res. Part C Emerg. Technol.* **2024**, *158*, 104411. [CrossRef]
23. Kim, G. Electric vehicle routing problem with states of charging stations. *Sustainability* **2024**, *16*, 3439. [CrossRef]
24. Nasehi, S.; Choudhury, F.; Tanin, E. Proactive Route Planning for Electric Vehicles. In Proceedings of the 32nd ACM International Conference on Advances in Geographic Information Systems, Atlanta, GA, USA, 29 October–1 November 2024; pp. 517–520.
25. Woo, S.; Choi, E.Y.; Moura, S.J.; Borrelli, F. Saving energy with eco-friendly routing of an electric vehicle fleet. *Transp. Res. Part E Logist. Transp. Rev.* **2024**, *189*, 103644. [CrossRef]
26. Huang, Y.-W.; Prehofer, C.; Lindskog, W.; Puts, R.; Mosca, P.; Kauermann, G. Predictive energy management for battery electric vehicles with hybrid models. In *International Conference on Intelligent Transport Systems*; Springer Nature: Cham, Switzerland, 2022; pp. 182–196.
27. Bao, W.; Kontou, E. Electric vehicle charging stations at risk from hazardous events and power outages: Analytics and resilience implications. *Renew. Sustain. Energy Rev.* **2026**, *226*, 116144. [CrossRef]
28. Sone, S.P.; Lehtomäki, J.J.; Khan, Z.; Umebayashi, K.; Kim, K.S. Robust EV scheduling in charging stations under uncertain demands and deadlines. *IEEE Trans. Intell. Transp. Syst.* **2024**, *25*, 21484–21499. [CrossRef]

Disclaimer/Publisher's Note: The statements, opinions and data contained in all publications are solely those of the individual author(s) and contributor(s) and not of MDPI and/or the editor(s). MDPI and/or the editor(s) disclaim responsibility for any injury to people or property resulting from any ideas, methods, instructions or products referred to in the content.